Hydrological Balance and its Variability over the Arid/Semi-arid Regions In the Eurasian Continent seen from Meteorological Reanalysis Data

Akiyo Yatagai
Research Institute for Humanity and Nature (RIHN), Kyoto, Japan
akiyo@chikyu.ac.jp

1. INTRODUCTION

Generally, environment of semi-arid regions are fragile and most of semi-arid regions in the world has a risk of desertification (UNEP, 1992). In most cases, desertification seems to be attributed to inappropriate human activities, however, some studies related with recent global warming issues pointed out a general drying of the mid-continental areas during summer. This is ascribed to a combination of increased temperature and potential evaporation that is not balanced by increases of precipitation (Wetherald and Manabe, 1999; IPCC, 2001).

While, it is important to grasp the current hydrological condition and its variability using the currently available meteorological reanalysis data to understand and validate the predicted future environment.

2. DATA AND ANALYSIS METHOD

We basically use the following the two datasets.

(1) European Centre for Medium-range Weather Forecasts (ECMWF) 15-year Re-Analysis (hereafter, ERA15) (Gibson et al., 1997). The ERA15 used here covers from 1979 to 1993, the temporal resolution is four times a day (00, 06, 12 and 18 UTC), and horizontal resolution is 2.5 degree by 2.5 degree (longitude/latitude). The original resolution of the ERA15 assimilation system used is T106. The upper-air and surface dataset of un-initialized analysis values are used.

(2) Climate Prediction Center Merged Analysis of Precipitation (CMAP) (Xie and Arkin, 1997). The 'rain 1' is used in order to avoid gaps. For consistency of the analyzing period, we also use this from 1979 to 1993.

The conservation of moisture vertically integrated from the top to the bottom can be expressed as

$$\partial W/\partial t = -\nabla\cdot[Q_\lambda, Q_\varphi] + E - P, \qquad (1)$$

where we have ignored other forms of liquid and frozen water in the atmosphere. E is the rate of evaporation and P represents precipitation; W is the precipitable water, and $[Q_\lambda, Q_\varphi]$ indicating the vertically integrated moisture flux vectors, that are defined by

$$W = \int_0^{Ps} q\,dp/g, \qquad (2)$$
$$Q_\lambda = \int_0^{Ps} qu\,dp/g, \qquad (3)$$
$$Q_\varphi = \int_0^{Ps} qv\,dp/g, \qquad (4)$$

and

$$\nabla\cdot[Q_\lambda, Q_\varphi] = 1/a\cos\varphi\ (\partial Q_\lambda/\partial\lambda + \partial Q_\varphi\cos\varphi/\partial\varphi) \qquad (5)$$

Since u, v, q, and Ps are all functions of time, Q_λ and Q_φ are evaluated four times daily data of ECMWF reanalysis. This computational procedure is the same as employed by Yatagai and Yasunari (1998). This is basically the same of atmospheric water balance method (e.g. Peixoto and Oort, 1983). The detailed computing scheme is the same as Oki et al. (1995) which evaluated hydrological budget using operational ECMWF datasets. The difference with them is to use 4-times ECMWF reanalysis, and to use surface dataset of ERA15.

By taking the climatological mean of each term in (1), we obtain

$$\langle E - P\rangle = \langle \nabla\cdot[Q_\lambda, Q_\varphi]\rangle, \qquad (6)$$

where the tendency term $\langle\partial W/\partial t\rangle$ was omitted.

The original paper was accepted to *Hydrological Processes* vol. 17(2003), titled "Hydrological Balance and its variability in arid and semi-arid regions of Eurasia form ECMWF 15-year Reanalysis" by A. Yatagai.

The <> indicates 15-year average. The equation (6) means that the climatological mean value of the vertically integrated evaporation minus precipitation can be estimated from the vertically integrated climatological mean moisture flux divergence .

The comparison of the $< \nabla \cdot [Q_\lambda, Q_\varphi] >$ with the precipitation field that is derived from 2. (CMAP precipitation) makes possible the evaluation of the evaporation field. We show the general in the next section on the features of $< E - P >$ in comparison with $< P >$ and estimated $< E >$ as the residual. However, we intend to focus on the characteristics of $< E - P >$ because our main concern here is the total surface moisture condition $< E - P >$, which is directory computed in the atmospheric water balance method, and P also includes various kind of errors.

3. GENERAL FEATURES

The moisture flux patterns of $[<Q_\lambda, Q_\varphi>]$ with precipitable water $<W>$ for the four representative month are shown in Fig.1. The precipitable water is less in the mountainous regions (Tibetan Plateau, Mongolian Plateau, Zagros mountains). Generally, western part of the Silk Road region is wetter than that in the eaastern part. In July, most region has the maximum precipitable water among the four panels (Figs.1 a)-d)). Roughly speaking, Moisture comes from the west to the Silk Road region, and the Mediterranean Sea is one of the strong moisture divergence (source) area all through the year.

However, in July, part of the eastern part of the Silk Road region receives moisture from the south. Over the Central Asia, moisture divergence with anti-cyclonic circulation around the Caspian Sea is observed, and moisture comes from northward (Fig.1c). While in April and October, the Central Asia receives moisture from the southwestward or southward. It seems the direction of water vapor flux is closely related with the location of pressure system.

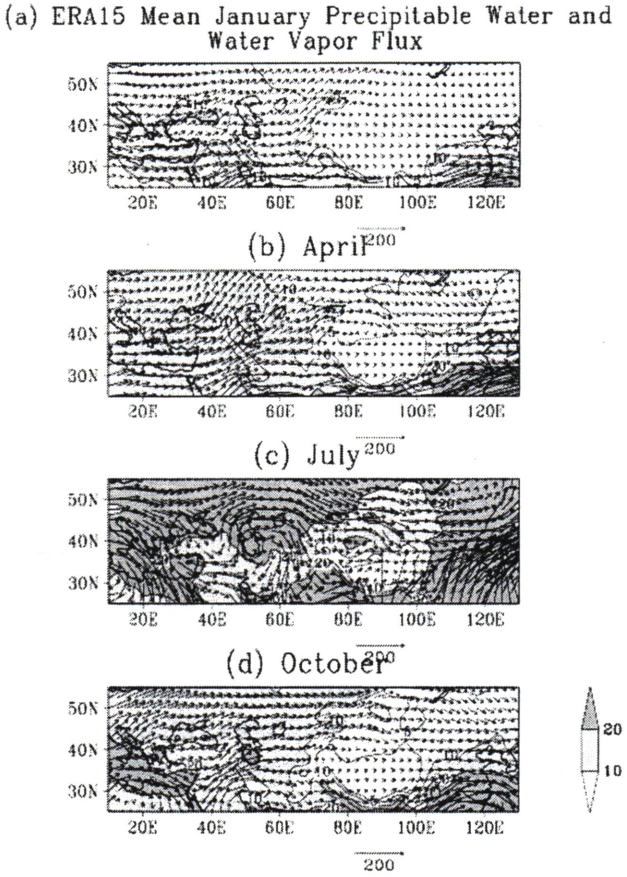

Fig. 1 Climatological mean $<W>$, $[<Q_\lambda, Q_\varphi>]$ in (a) January, (b) April, (c) July and (d) October. Units of $<W>$ is mm, and regions with more than 10 mm are shaded. The unit vector of $[<Q_\lambda, Q_\varphi>]$ is shown in the diagram and the unit is mm x m/s.

4. AREAL AVERAGES

In order to better understanding of the hydrological regimes and their seasonal variation in the Silk Road

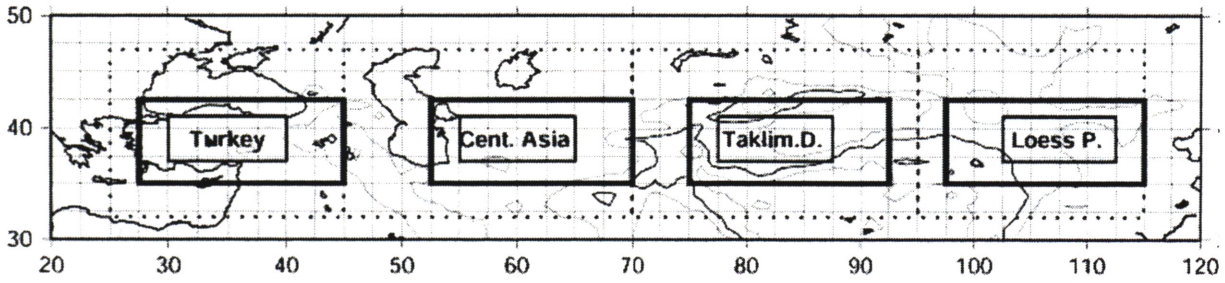

Fig. 2 Geographical distributions of the target box regions. Each inner box represents small region (S), larger boxes with thicker straight lines represent medium regions (M), the largest dotted boxes mean the largest regions (L) in this study. The geographical contours in 1,500 m and 3,000 m are also displayed.

region, the region is divided into the four sub-regions as shown in Fig.2. Among three size of boxes, we present the results of medium-size regions (M) in Fig.2. Averaging the $<-\nabla\cdot[Q_\lambda, Q_\varphi]>$ (moisture convergence), and CMAP $<P>$ over (a) Turkey, (b) Central Asia, (c) Taklimakan Desert, and (d) Loess Plateau for each calendar month yields the profiles shown in Fig.3. As one would expect, in most cases, there are good qualitative agreement between the convergence and precipitation maxima.

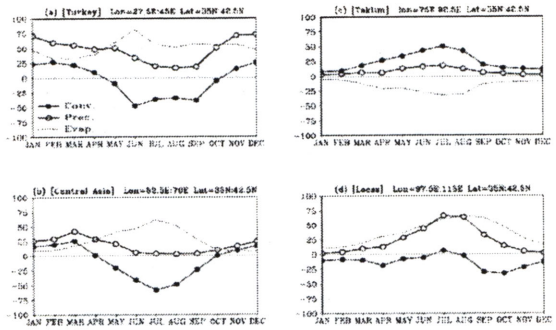

Fig. 3 Annual cycle of $<-\nabla\cdot[Q_\lambda, Q_\varphi]>$ (moisture convergence = C), and CMAP $<P>$ for the Silk Road subregions (a) Turkey, (b) Central Asia, (c) Taklimakan Desert, and (d) Loess Plateau, in units of mm/month. Averaged domains are shown on the each panel and in Fig.2 (medium regions). The thick straight lines with closed circles represent moisture convergence, while those with open circles represent precipitation. The dashed lines mean estimated evaporation by $<-\nabla\cdot[Q_\lambda, Q_\varphi]>$ - $<P>$..

Over the Taklimakan Desert, the Convergence > Precipitation, which means it does not consistent relationships. In all sub-regions, we can see reasonable and consistent seasonal variation. In Turkey, convergence maximum is observed in February, while precipitation is near peak from November to January. In the M-size region, divergence has two peaks in June and September, while if it is average in L-size region (cf. Fig.2), the divergence and precipitation show smooth curves.

Over the Central Asia, both precipitation maximum and the strongest convergence are seen in March. As we see in Fig.1, this sub-region is moisture divergence from May to September, and the July divergence is the largest amoung the four sub-regions and all months.

Over the Taklimakan Desert, both precipitation and convergence maximum are appeared in July. As for the erroneous evaporation, it is appeared if we take L-size sub-region (cf. Fig.2, figure not shown).

Over the Loess Plateau, precipitation maximum appears in July. For convergence, relative peak appears also in July, but the range of seasonal cycle of convergence/divergence is small comparing to other regions. The evaporation peak appears in August, and the curve follows those of precipitation and convergence. It is a different feature with Tureky and Central Asia, where evaporation peak consistent with divergence peak.

5. INTERANNUAL VARIABILITY

The interannual variability of moisture flux and its divergence is investigated for each sub-region. Here we display moisture budget diagrams for convergence maximum months for each sub-region.

The moisture budget over Turkey in February and Central Asia in March are almost alike, with southerly flow in Turkey is stronger than that in Central Asia.

In July, the moisture budget over Taklimakan and Loess are qualitatively similar. However, all moisture fluxes around Taklimakan are relatively small comparing those around Loess Plateau. Over the Taklimakan Desert, moisture from the south is quite few, because of there exist Tibetan Plateau. In Yatagai and Yasunari (1998), sometimes strong moisture form the south is denoted over the Taklimakan. These contradict are attributed from the region we defined. Here we defined the sub-region from 92.5E to the west, and this does not include moisture from the eastern Tibetan Plateau.

6. REFERENCES

Gibson JK, Kallberg P, Uppala S, Nomura A, Hernandez A, and Serrano E. 1997. ERA Discription. *ECMWF re-analysis project report series*, **1**, 72pp.

IPCC. 2001. Climate Change 2001: The Scientific Basis. Houghton J.T., Ding Y., Griggs D.J., Noguer M., van der Linden P.J., Dai X., Maskell K., Johnson C.A. (eds.), Cambridge, UK, 881pp.

Oki T, Musiake K, Matsuyama H, Masuda K, 1995. Global atmospheric water balance and runoff from large river basins. *Hydrological Processes*, **9**: 655-678.

Peixoto JP, Oort AH. 1983. The atmospheric branch of the hydrological cycle and climate. *Variation in the*

Global Water Budeget, A. Stret-Perrott and Co-editors, D. Reidel, 5-65.

UNEP. 1992. *World Atlas of Desertification*, Edward Arnold, 70pp.

Wetherald RT, Manabe S. 1999. Detectability of summer dryness caused by greenhouse warming. *Climatic Change*, **43**: 495-511.

Xie P, Arkin PA. 1997. Global precipitation: A 17-year monthly analysis based on gauge observations, satellite estimates, and numerical model outputs. *Bull. Amer. Meteorol. Soc.*, **78**: 2539-2558.

Yatagai A, Yasunari T. 1998. Variation of Summer Water Vapor Transport over and around the Arid Region in the Interior of the Eurasian Continent. *J. Meteor. Soc. Japan*, **76**: 799-815.

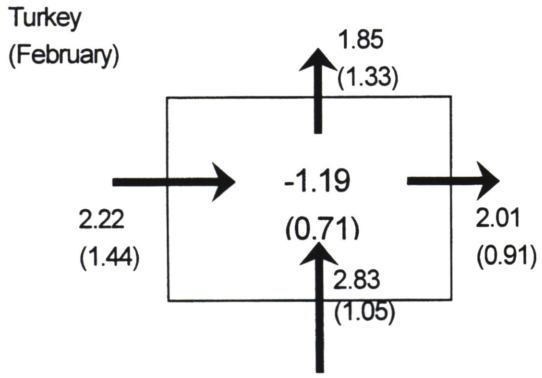

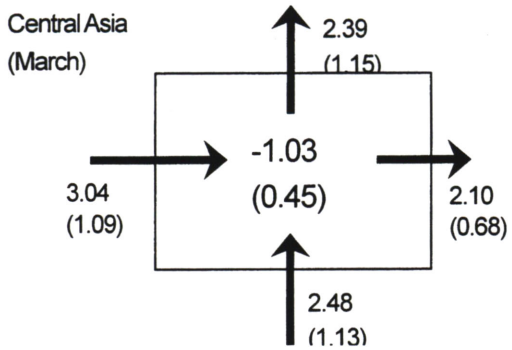

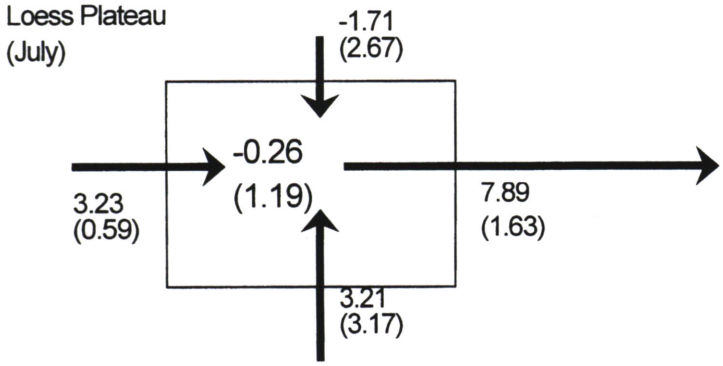

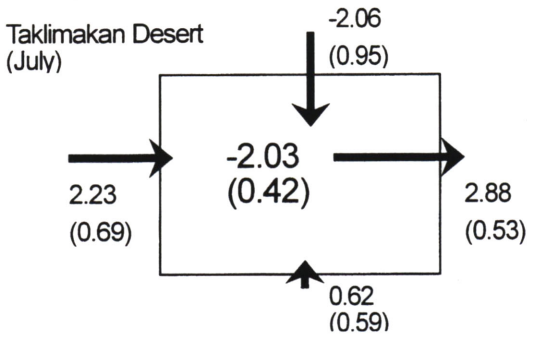

Fig. 3 Intetannual variability of moisture budget over (a) Turkey in February, (b) Central Asia in March, (c) Loess Plateau in July and (d) Taklimakan desert in July. The positive (netative) numbers mean eastward (westward) flow, northward flow (southward), or moisture divergence (convergence). The numbers in the ( ) mean standard deviation.

The original paper was accepted to *Hydrological Processes* vol. 17(2003), titled "Hydrological Balance and its variability in arid and semi-arid regions of Eurasia form ECMWF 15-year Reanalysis" by A. Yatagai.